ACS NANO

www.acsnano.org

ARTICLE

Dual-Purpose Aptamer-Based Sensors for Real-Time, Multiplexable Monitoring of Metabolites in Cell Culture Media

Yiling Yang, Xumei Gao, Bryce Widdicombe, Xiaodan Zhang, Jana Lorraine Zielinski, Tianhong Cheng, Avanka Gunatilaka, Kaylyn K. Leung, Kevin W. Plaxco, Ranjith Rajasekharan Unnithan,* and Alastair G. Stewart*

Cite This: *ACS Nano* 2024, 18, 26127−26139

Read Online

ACCESS | Metrics & More | Article Recommendations | Supporting Information

ABSTRACT: **The availability of high-frequency, real-time measurements of the concentrations of specific metabolites in cell culture systems will enable a deeper understanding of cellular metabolism and facilitate the application of good laboratory practice standards in cell culture protocols. However, currently available approaches to this end either are constrained to single-time-point and single-parameter measurements or are limited in the range of detectable analytes. Electrochemical aptamer-based (EAB) biosensors have demonstrated utility in real-time monitoring of analytes *in vivo* in blood and tissues. Here, we characterize a pH-sensing capability of EAB sensors that is independent of the specific target analyte of the aptamer sequence. We applied this dual-purpose EAB to the continuous measurement of pH and phenylalanine in several *in vitro* cell culture settings. The miniature EAB sensor that we developed exhibits rapid response times, good stability, high repeatability, and biologically relevant sensitivity. We also developed and characterized a leak-free reference electrode that mitigates the potential cytotoxic effects of silver ions released from conventional reference electrodes. Using the resulting dual-purpose sensor, we performed hourly measurements of pH and phenylalanine concentrations in the medium superfusing cultured epithelial tumor cell lines (A549, MDA-MB-23) and a human fibroblast cell line (MRC-5) for periods of up to 72 h. Our scalable technology may be multiplexed for high-throughput monitoring of pH and multiple analytes in support of the broad metabolic qualification of microphysiological systems.**

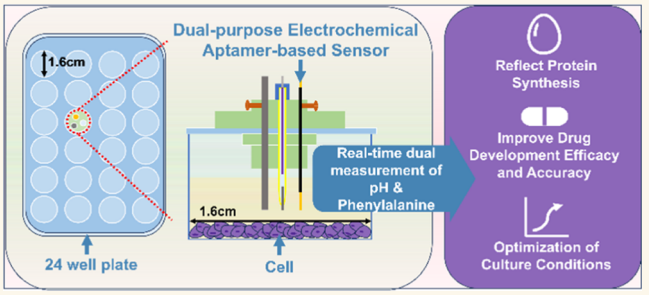

KEYWORDS: *biosensor, microphysiological system, organ-on-a-chip, pH-sensor, phenylalanine, cell metabolism, real-time monitoring*

Conventional drug discovery and development require preclinical research, including *in vitro* studies (cell culture studies) and *in vivo* studies (animal models).[1,2] However, limitations in the (patho) physiological accuracy of both cell culture and experimental animals as models of human patients lead to the qualification of many drug candidates as efficacious and safe that fail during clinical trials.[3] In response to this deficiency in disease modeling, microphysiological systems (MPS) of increasingly tissue- and organ-like complexity are being developed for *in vitro* drug evaluation.[4−6] Such MPS encompass the use of multiple organ-on-a-chips, facilitating functional connections among organs such as the liver,[7,8] brain,[9,10] lung,[11,12] and bone[13] and even more complex multiorgan systems[14−16] by using human cells cultured from tissues or obtained from differentiation of induced pluripotent stem cells. These MPS advances have required innovation in fabrication in both the open tissue culture plate setting and the microfluidic system setting. However, because innovations in real-time molecular monitoring of the cell culture medium are limited to date, the ability to monitor the (super) perfusate metabolite composition in such systems is largely lacking.

The ability to perform real-time, high-frequency metabolic monitoring in MPS would (1) improve our understanding of cell metabolism and how this is modulated by drug candidates, (2) enable feedback control of the metabolic environment in the MPS, and (3) support the high-precision optimization of cell-culture protocols.[17] Coupled with the advancement of real-

Received: May 22, 2024
Revised: August 27, 2024
Accepted: August 29, 2024
Published: September 10, 2024

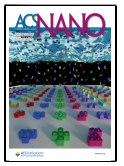

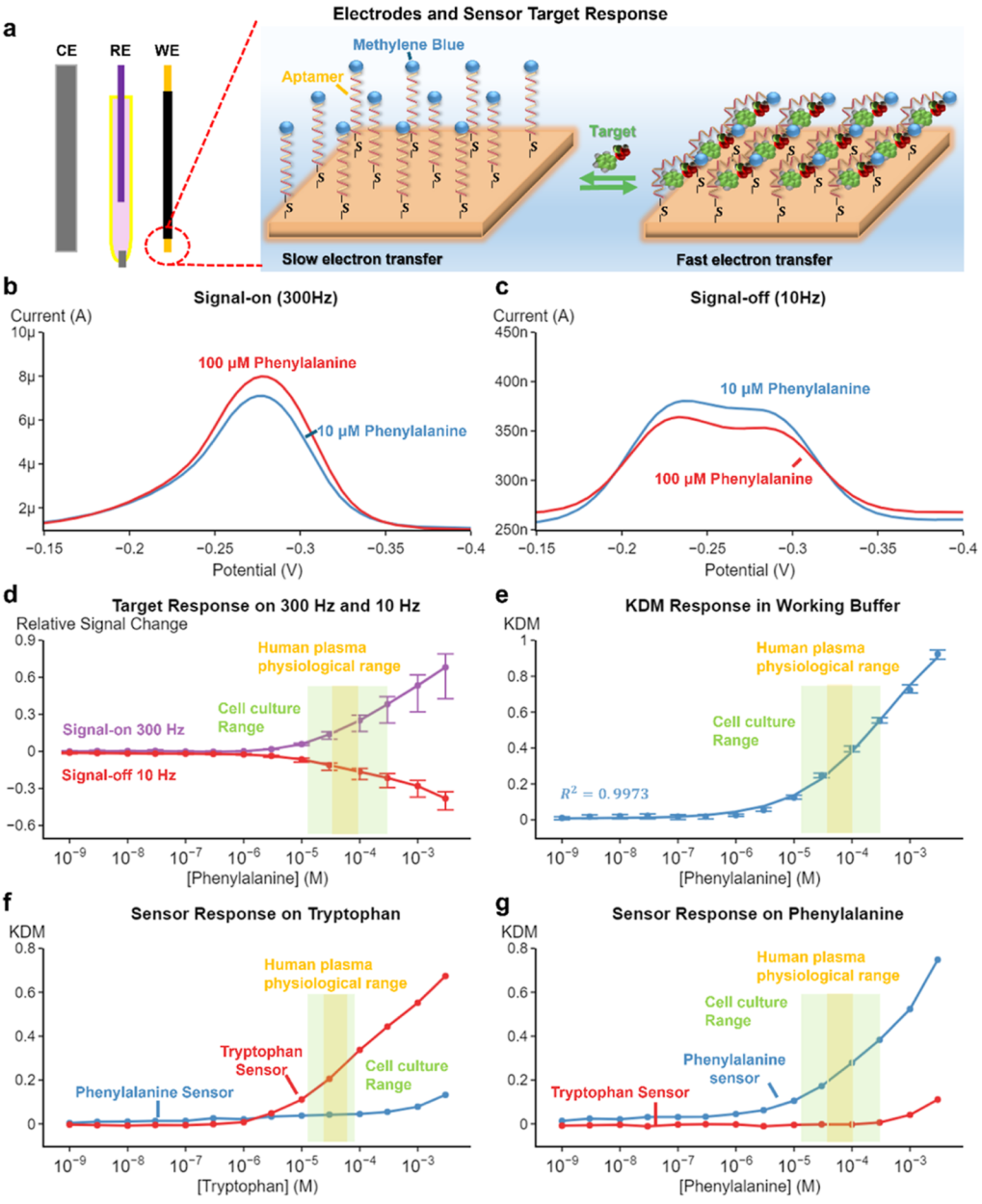

Figure 1. Characterization of aptamer sensor target metabolite measurement. (a) Aptamer sensor molecular structure changes upon target metabolite binding. (b) Plot of single signal-on (300 Hz) SWV scan results. (c) Plot of single signal-off (10 Hz) SWV scan results. (d) Signal-on and signal-off signal change ratio over phenylalanine concentration varied from 1 nM to 3 mM in working buffer (n = 4). (e) Kinetic differential measurement (KDM) response curve over phenylalanine concentration varied from 1 nM to 3 mM in working buffer (n = 4); the error bars are the maximum and minimum values over these 4 independent gold electrode measurements, and the orange shaded area is the human plasma physiological phenylalanine range of 50−100 μM.[48,49] (f) Selectivity analysis plot against tryptophan concentrations; the orange shaded area is the human plasma physiological tryptophan range of 40−70 μM.[48,49] (g) Selectivity analysis plot against phenylalanine concentrations; the orange shaded area is the human plasma physiological phenylalanine range.

time monitoring, this capability will render MPS more human-like than conventional cell culture models. To date, such metabolite monitoring usually has relied on liquid chromatography−mass spectrometry (LC−MS) or high-performance liquid chromatography, which are multistep, "batch" processes that do not support real-time or high-frequency monitoring.[18] In contrast, biosensors, which measure target concentrations via metabolite interacting with a receptor to generate an optical[19,20] or electronic signal,[21−23] potentially offer a means of continuous, real-time monitoring of cell metabolism. However, optical methods are often limited by the perturbation of the culture due to optical reporter (bio)-chemistry, such as the estrogenic activity of the pH sensor phenol red.[24] In contrast, electrochemical sensors often perform well in complex media and generally do not perturb the media. Electrochemical methods have been used in real-time sensing in MPS. To date, however, the range of measurements reported is limited to oxygen,[19,21,23,25] glucose,[22,23] lactate,[22,23] and pH.[26] This leaves many important metabolites unaddressed. For example, the monitoring of amino acids has yet to be established, even though amino acid concentrations in cell culture medium are critical to protein

https://doi.org/10.1021/acsnano.4c06813
ACS Nano 2024, 18, 26127−26139

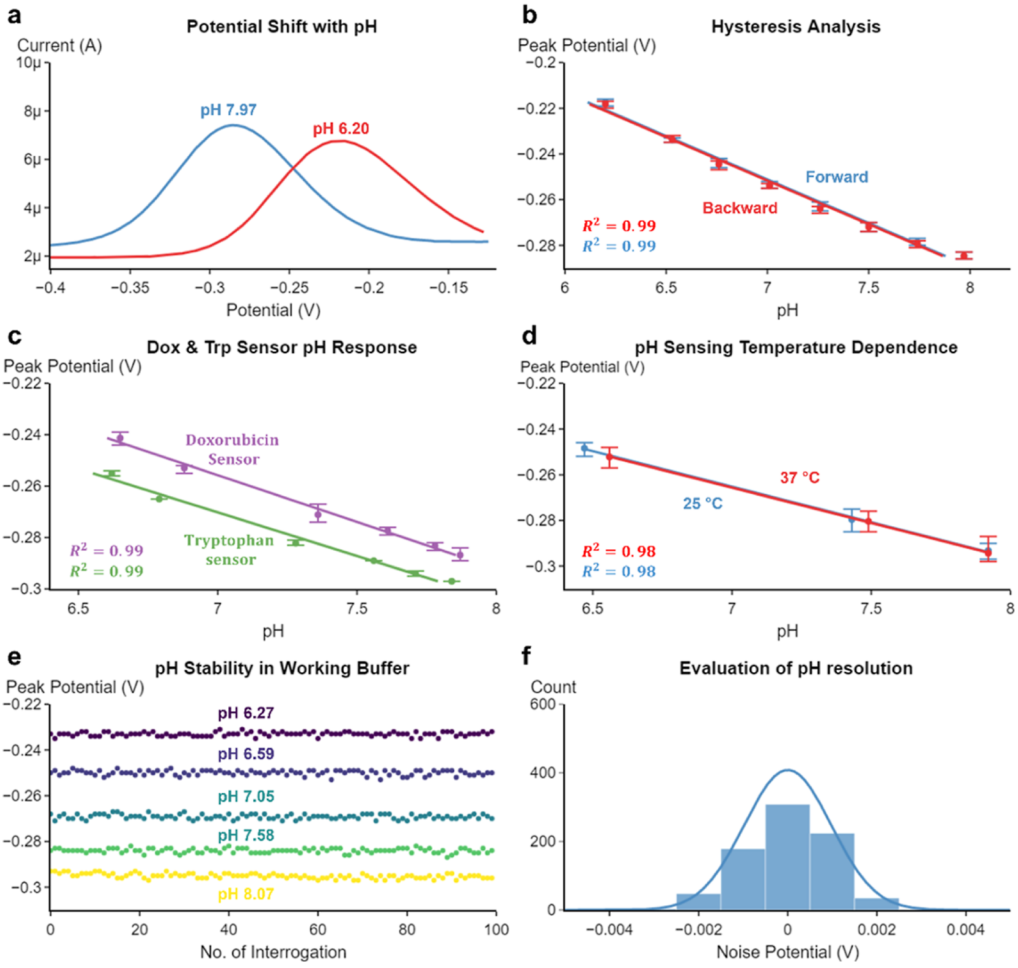

Figure 2. Characterization of sensor pH measurement. (a) Plot of single signal-on SWV scan results over different pH conditions. (b) pH hysteresis analysis curve between pH 6 and pH 8. (c) pH response curve over pH changes from 6 to 8 with doxorubicin sensor and tryptophan sensor. (d) pH response curve under ambient temperature (25 °C) and incubator temperature (37 °C). (e) Stability of peak potential over multiple measurements (100 measurements per pH). (f) Estimation of pH measurement accuracy over 500 data points based on measured noisesl; the fitting curve was based on Gaussian distribution. All error bars are the maximum and minimum values over 10 continuous measurements.

production[27] and cell growth.[28] Amino acids influence tumor cell survival.[29−31] Thus, variability in amino acid availability in "uncharacterized" cell culture media may increase both variability and confounding in cell culture experiments focused on tumor biology or drug discovery. Thus, the capability to qualify and control amino acid levels in cell culture media would address a critical limitation in the reproducibility and predictive value of cell culture studies in drug discovery/development.

We have adapted an electrochemical aptamer-based (EAB) sensor to address the need for a more broadly applicable, potentially multiplexable method of monitoring the composition of media in MPS. The EAB sensor uses aptamers that comprise oligonucleotides selected for their selective binding of target molecules with useful affinity[32] to perform real-time, high-frequency measurements. A wide range of metabolites, such as phenylalanine[33] and adenine triphosphate,[34] and drugs, such as doxorubicin,[35] vancomycin,[36] irinotecan,[37] methotrexate,[38] and procaine,[39] have been measured in complex sample matrices, including in tissues and blood of living rats. Given this range of usage, we considered that EAB sensors could be adapted to the cell culture/MPS environment to advance our understanding of the pharmacodynamics and pharmacokinetics of drugs in environments that are more *in vivo*-like than those used in conventional cell culture studies.

For the adaptation of the EAB to the cell culture environment, we chose the essential amino acid phenylalanine as the target analyte because the phenylalanine sequence used has been well-characterized,[33] phenylalanine is a critical influence on many processes, including proliferation of multiple myeloma cells,[40] and in genetic diseases, such as phenylketonuria.[41,42] Moreover, phenylalanine production using biotechnologies, such as microbial fermentation, may be facilitated by real-time phenylalanine measurement. We identified the necessity to develop a cell culture medium to enable adjustment of each analyte concentration for sensor calibration, as no commercially available cell culture medium affords this control over the medium amino acid composition. The cell culture medium based on the design principle of mimicking plasma ultrafiltrate known as the "Melbourne Medium" also provides a more physiological approach to understanding amino acid function and indeed provides a more physiological environment for cell culture/MPS. The dual-purpose EAB sensor was miniaturized for use in multiwell plate cell culture systems and fabricated with the leakless reference electrode[43] to mitigate the potential cytotoxicity of

https://doi.org/10.1021/acsnano.4c06813
ACS Nano 2024, 18, 26127−26139

silver ion leakage from conventional reference electrodes. In the breadth of our characterization of the dual-purpose EAB in media of different pH values, we also discovered that the electronic features of the methylene blue-containing aptamer sequence sense pH in a target analyte-independent manner, providing a dual-purpose EAB technology.

RESULTS AND DISCUSSION

Characteristics of EAB Sensors. In this study, we have used a previously characterized phenylalanine aptamer to establish EAB operationally in cell culture environments. The core elements of an EAB sensor comprise three electrodes: a platinum counter electrode, a silver/silver chloride reference electrode, and a gold working electrode. The latter incorporates a self-assembled monolayer modified with a submonolayer of aptamer and affixed via a gold−sulfur bond. The distal terminus of the aptamer is covalently modified with a redox reporter (here, methylene blue). Upon interaction with the target, the aptamer undergoes a conformational change that alters the distance between the methylene blue and the electrode, thereby influencing the rate of electron transfer (Figure 1a). To detect this change in electron transfer rate, we employ square wave voltammetry (SWV).[33,36,44] We initially characterized the phenylalanine (target analyte) EAB sensor by SWV in a simple buffer devoid of amino acids ("working buffer"). The phenylalanine EAB sensor showed increasing peak current differences with increasing phenylalanine concentrations at a "signal-on" square-wave frequency of 300 Hz (Figure 1b), and, conversely, a decrease in peak current differences with increasing phenylalanine concentrations at a "signal-off" frequency of 10 Hz (Figure 1c), as previously reported.[33]

The phenylalanine EAB sensor responds over the entire physiologically relevant concentration range of phenylalanine. The signal-on frequency (300 Hz) current differences relative signal change and signal-off frequency (10 Hz) current differences relative signal change both showed responses at 400 μM phenylalanine concentrations encountered in Dulbecco's modified Eagle medium (DMEM) and at 80 μM concentrations used in Human Plasma Like Medium (Figure 1d). To achieve higher accuracy in detection of phenylalanine and to correct for any sensor drift,[33,38,45] we combined the signals measured at signal-on and signal-off frequencies to calculate the KDM.[33,38,45] We fitted KDM to the Langmuir−Hill equation[46] displaying high goodness of fit $\left(\mathrm{KDM} = 0.0066 + \frac{(1.1874 - 0.0066) \times \mathrm{Phe}^{0.5711}}{\mathrm{Phe}^{0.5711} + 0.0004^{0.5711}} \quad (R^2 \text{ and with } = 0.9973)\right)$ the slope covering the phenylalanine concentration range relevant for use in measuring cell culture media (Figure 1e). Thus, we established that the sensor response to phenylalanine in the human plasma physiological range in working buffer at room temperature (20−25 °C) is accurate to 10% (i.e., KDM standard deviation less than 10% between 10 and 100 μM).

To confirm the selectivity of the sensor and the potential to multiplex these devices, we also fabricated EAB sensors against tryptophan.[47] We observe only negligible cross-reactivity between the two sensors over ranges of concentrations of the respective target analytes relevant to human plasma (Figure 1f,g).[48,49]

EAB Sensor Shows Linear pH-Related Shifts in Peak Voltage. A routine characterization of the aptamer sensor in working buffer adjusted to different pH values revealed that the peak potential changed with the changes in pH (Figure 2a). The pH-sensing properties of methylene blue have previously been reported,[50,51] and exploited in pH sensors, using both optical[52] and electrochemical methods,[53] although not when coupled to an aptamer. We characterized the phenylalanine EAB sensor pH sensing capability in the physiological pH range of 6−8 by sequentially placing the EAB sensors in solutions of pH from low to high (forward) and then from high to low (backward) (Figure 2b). A near perfect linear relationship was obtained with no evidence of hysteresis, yielding the equation with 95% confidence intervals: peak potential (V) = −(0.038 ± 0.004) × pH + (0.012 ± 0.027) (R^2 = 0.99), and reverse curve with equation: peak potential (V) = −(0.038 ± 0.004) × pH + (0.012 ± 0.028) (R^2 = 0.99) (Figure 2b). To assess the generalizability of the pH sensing, we characterized the pH response of two other EAB sensors, one targeting doxorubicin and the other tryptophan. The doxorubicin EAB sensor equation with 95% confidence intervals is peak potential (V) = −(0.036 ± 0.004) × pH + (0.003 ± 0.032) (R^2 = 0.99); and the tryptophan EAB sensor equation showing ±95% confidence intervals is peak potential (V) = −(0.034 ± 0.005) × pH + (0.004 ± 0.039) (R^2 = 0.99). Both the tryptophan EAB sensor and the doxorubicin EAB sensor showed linear pH response curves, supporting the conclusion that pH sensing properties are likely a generic feature of EAB sensors using a methylene blue reporter (Figure 2c).

The pH detection capability of the EAB sensor demonstrated insensitivity to temperature variations and achieved a resolution better than 0.1 pH units within the physiological pH and temperature ranges of human plasma. Working buffers with different pH levels at 37 °C were transitioned to 25 °C to assess the impact on pH measurement. 37 °C results were fitted to a linear regression equation with 95% confidence intervals: peak potential (V) = −(0.031 ± 0.002) × pH − (0.047 ± 0.013) (R^2 = 0.98), as were 25 °C results: peak potential (V) = −(0.031 ± 0.002) × pH − (0.050 ± 0.014) (R^2 = 0.98) (Figure 2d). The overlapping regression lines indicate that pH sensing in the range 25−37 °C (cell culture temperature) is effectively temperature-independent (Figure 4f). To establish the pH resolution of the sensor, we placed the EAB sensor in working buffer at 6 different pH values with a scanning frequency of 300 Hz (0.0033 s for each measurement). The measured peak potential showed stability at each pH value (Figure 2e). We fitted these absolute noise values to a Gaussian distribution (Figure 2f), which showed a mean (0.0152 fV) and standard deviation (0.98 mV). From the absolute noise values, we estimated the resolution based on the 3-sigma law (99.7% estimation accuracy) in the working buffer to be 0.086. Moreover, this resolution could readily be further improved by averaging longer sampling periods.

Miniaturized, Leakless Reference Electrode. To adapt EAB sensors for monitoring metabolism in cell culture requires (1) miniaturization of the three electrodes to fit within the culture well, (2) the ability to sterilize the device prior to use, and (3) biocompatibility with the cultured cells. Regarding the latter point, silver ions or silver nanoparticles from a conventional Ag/AgCl reference electrode may interact with metabolic enzymes,[54] nucleic acids[55] to perturb biomolecular cell function with cytotoxic potential.[56] The porous frit was

https://doi.org/10.1021/acsnano.4c06813
ACS Nano 2024, 18, 26127−26139

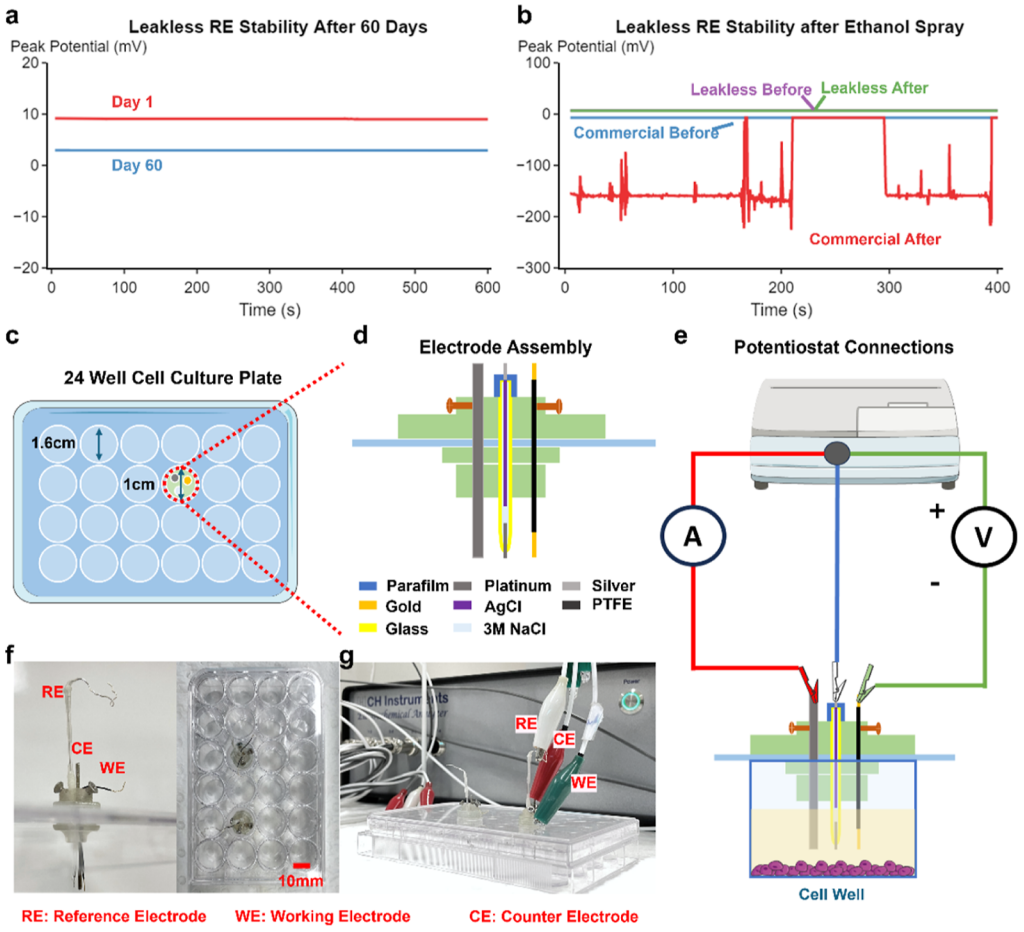

Figure 3. Cell culture sensor system. (a) Leakless reference electrode potential longevity measurement. (b) Leakless reference electrode potential and commercial reference electrode potential differences before and after ethanol (80%) spray. (c) Overview of 24-well sensor lid. (d) Schematic of cell well sensor element consisting of three electrodes vertically inserted into the well lid. (e) Schematic of sensor system electrical connections with potentiostat and the sensor position to biological sample. (f) Side view and top view of sensor element installed on commercial culture plate lid. (g) Prototype of the sensor electrical interface to the commercial potentiostat.

adapted in a commercial reference electrode to mitigate the leaking silver ion, but those are too bulky (~10 mm) to integrate into a culture well (15.6 mm). Thus, we used a recently reported miniaturized leakless reference electrode design to overcome the potential issue of silver ion cytotoxicity while retaining the advantages of miniaturization and longer shelf life.[43] To make the leakless reference electrode, the glass capillary tube was sealed at one end with the platinum wire to prevent leakage of silver ions while also ensuring charge balance through the movement of electrons[43] (Figure S3). The inside of the glass capillary tube was filled with 3 M NaCl to ensure that the potential of the Ag/AgCl electrode remains stable and reproducible over time. Open circuit potential measurement was obtained in 3 M NaCl to compare the leakless electrode against a commercial reference electrode (BASMF2052). To evaluate shelf life, we stored the fabricated leakless reference electrode in an ambient environment for over two months and then compared its open-circuit potential against that of a commercial reference electrode. The results showed leakless electrodes remained relatively stable, drifting by less than 7 mV over 2 months (Figure 3a). Besides avoiding silver ion leaking and increasing shelf life, the importance of a leak-free reference electrode is further underscored by the necessity for sterilization methods in cell culture environments. Ethanol (70−80% v/v) is commonly the sterilization method of choice for laboratory equipment used in biosafety environments. To check the compatibility of this sterilization method with our leakless reference electrode, we first took open circuit potential measurements using the leakless reference electrode and the commercial reference electrode before spraying each with a sterilizing solution of 80% v/v ethanol. The comparison of the subsequent open circuit potential measurements established that the leakless potential was unaffected by the ethanol spray, whereas the commercial reference potential became unstable (Figure 3b).

Tissue Culture Plate Compatible Sensor. Integrating the EAB sensor into multiwell culture plates also requires consideration of the potential to physically damage the confluent layer of cells. We integrated the three electrodes into a single well (15.6 mm diameter) of the 24-well plate (CoStar, Washington, USA) to afford a more user-friendly and standardized assembly that precludes damage to the cells. A 3D-printed sensor holder was prepared from biocompatible transparent resin to fix the three electrodes. A 1 cm diameter hole was punched in the middle well to allow for the insertion of the 3D-printed sensor holder (Figure 3c). The leakless reference electrode was sealed with parafilm to prevent evaporation of the 3 M NaCl solution (Figure 3d). The final culture plate-sensor assembly prevents direct contact between

https://doi.org/10.1021/acsnano.4c06813
ACS Nano 2024, 18, 26127−26139

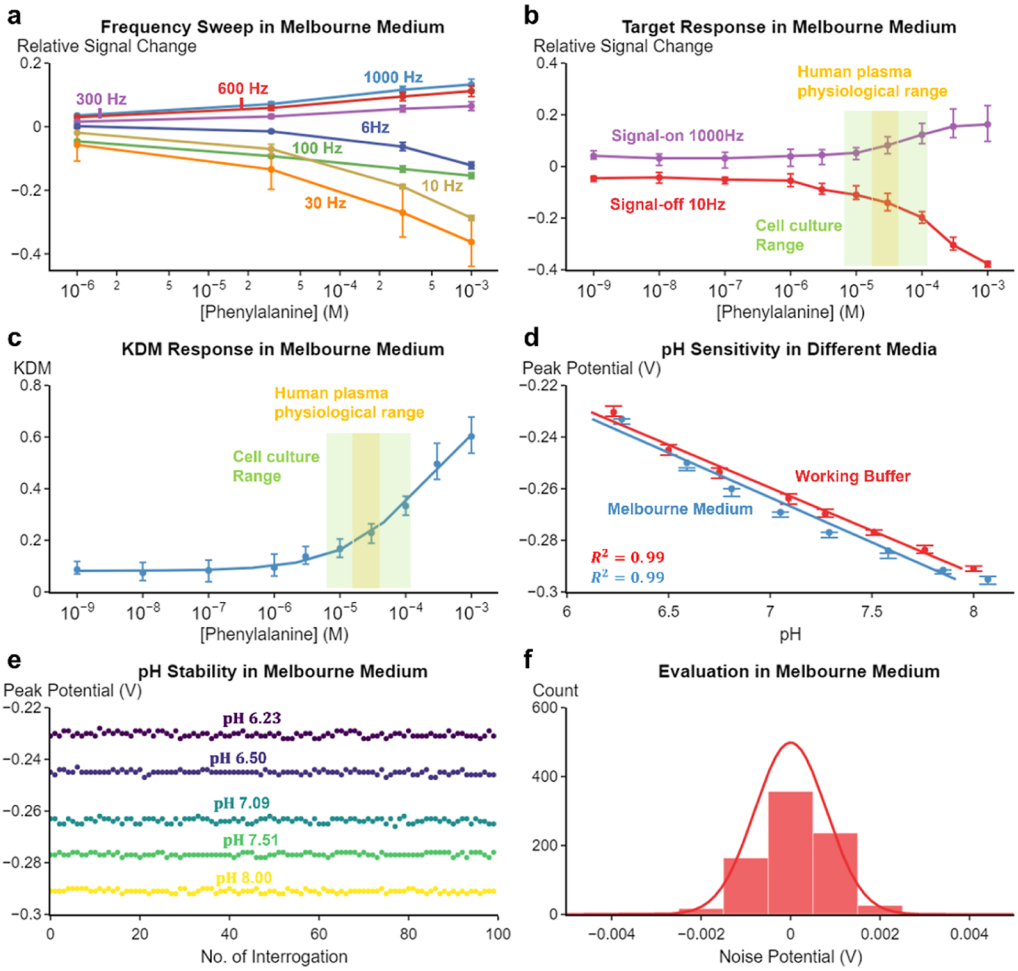

Figure 4. Characterization of sensor and leakless reference electrode under cell culture conditions. (a) Sensor frequency sweep in physiological medium [Melbourne Medium (MM)]. (b) Signal-on and signal-off signal change ratio over phenylalanine concentration varied from 1 nM to 3 mM in MM (n = 3). (c) KDM response over phenylalanine concentration varied from 1 nM to 3 mM in MM (n = 3). (d) pH sensitivity comparison in working buffer and MM. (e) pH measurement stability in MM. (f) Sensor pH resolution estimation in MM. All error bars are the maximum and minimum values.

the sensor and the cell monolayer, thus avoiding the sensor scratching the cell layer (Figure 3e).

EAB Sensor Measurement in Cell Culture Environment. The EAB sensor has been characterized in a human plasma-like medium environment. All prior calibration and fabrication processes were conducted in ambient environments, whereas mammalian cell culture is conventionally conducted at 37 °C. Considering temperature-dependent affinity variation of the EAB sensor,[57,58] we calibrated the sensor in the cell culture setting, which required customization of metabolite concentrations in the media. Conventional commercial cell culture media lack the required flexibility for controlling phenylalanine concentrations, particularly within the human plasma range, as commonly used media contain excessive concentrations of phenylalanine and most other amino acids. We developed the "Melbourne Medium" (MM), a culture medium with specified plasma-like nutrient concentrations (Tables S1−S3) to mimic plasma composition and enable control of the concentrations of individual components. During the course of our work, commercial plasma-like media became available, but these media (Plasmax and Human Plasma Like) do not offer the control over composition, being supplied in a finally constituted format precluding, for example, the independent adjustment of phenylalanine or tryptophan concentrations, as is required in the current work. MM is prepared from constituent components and therefore offers full control over component concentrations, which further supports its strategic utility for feedback control superfusion of MPS. Initial attempts to calibrate the phenylalanine concentrations in MM used the same scanning frequency as used for working buffer, but with the sensor in an incubator (37 °C, 5% CO_2). The EAB sensor signal change seen at a square-wave frequency of 300 Hz reached a plateau at lower phenylalanine concentrations than was observed in simple buffer (Figures S1 and S2), reducing the sensor dynamic range and thus its utility. Given this, we re-examined a range of signal-on frequencies, concluding that 1000 Hz is optimal (Figure 4a). A titration study employing this frequency (Figure 4b,c) confirmed that using a square-wave frequency of 1000 Hz provides higher stability and improved sensitivity relative to 300 Hz.

We further characterized the pH sensing in a cell culture environment. Immersion of the EAB sensor in the working buffer or MM showed similar pH response: working buffer equation: peak potential (V) = $-(0.034 \pm 0.006) \times$ pH + (-0.028 ± 0.042) (R^2 = 0.99); MM equation: peak potential (V) = $-(0.033 \pm 0.003) \times$ pH + (-0.03 ± 0.024) (R^2 = 0.99) (Figure 4d). We further confirmed the sensor pH measure-

https://doi.org/10.1021/acsnano.4c06813
ACS Nano 2024, 18, 26127−26139

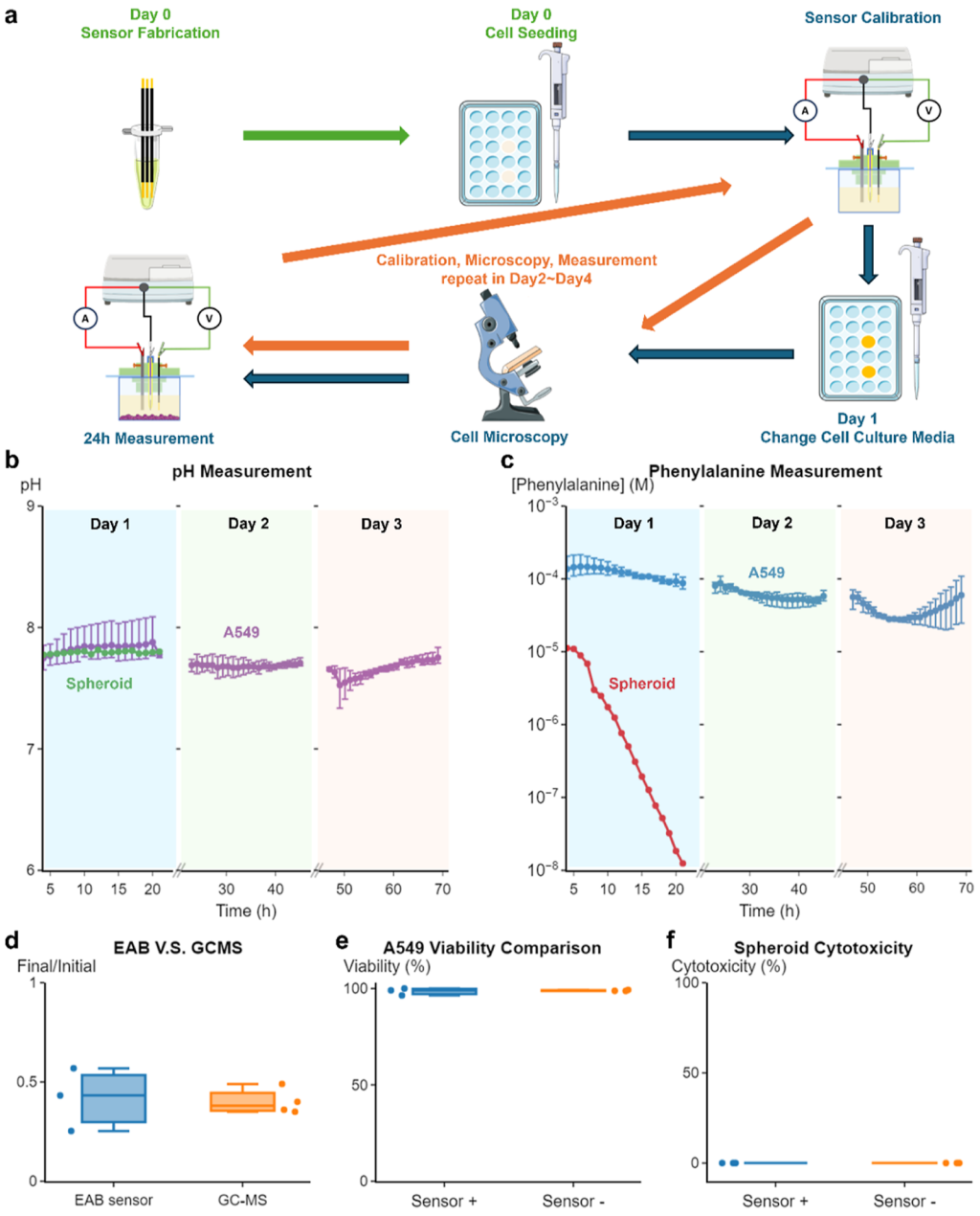

Figure 5. Cell metabolic measurements in the sensor system. (a) Methods and workflow diagram for cell metabolic condition monitoring. (b) Continuous pH measurement of A549 cell culture (n = 3) and the MRC-5 fibroblast spheroid. (c) Phenylalanine measurement of A549 cell culture (n = 3) and spheroid. (d) Final point and initial point ratio comparison between the EAB sensor (n = 3) and GC−MS (n = 4). (e) A549 viability comparison between the cell well with sensor and without sensor (n = 3). (f) Spheroid cytotoxicity comparison between the cell well with sensor and without sensor. All error bars are the maximum and minimum values.

ment resolution and stability by placing the sensor in a MM to assess noise in pH measurement (Figure 4e). The fitted mean is close to 0 (0.020 fV) with a standard deviation of 0.8 mV. We estimated that the pH resolution in MM is 0.071 pH units (Figure 4f).

EAB Sensor Performance in Flowing Media. We evaluated the sensor stability at different flow rates by fabricating a 3D printed culture well and culture lid with five holes, two of which are situated at opposite edges of the well, providing inflow and outflow connections (Figure S4). The three sensor electrodes penetrate the lid through the central holes (Figure S5). We interrogated the sensor with 30−60 scans until the sensor signal stabilized, then started 10 groups of SWV scans with a frequency of 300 Hz (which is appropriate for the working buffer used in these studies) and changed the flow rate from lower to higher (forward) and back from high to low (backward). The measured SWV peak potential versus flow rate change was less than 1 mV (Figures S6 and S7), and the measured KDM versus flow rate change was less than 0.01 (Figures S8 and S9), indicating that sensor pH performance and target analyte performance were independent of relevant flow rates. Thus, the EAB sensor performs well in the flowing media, establishing the potential for the sensor to be used in perfused systems.

Assessing Cellular Metabolism. The EAB sensor has undergone testing and benchmarking to assess its effectiveness in real-time evaluation of the cellular metabolism. Culture medium pH and phenylalanine levels were assessed at 37 °C,

https://doi.org/10.1021/acsnano.4c06813
ACS Nano 2024, 18, 26127−26139

5% CO_2. A549 cells (adenocarcinoma-derived human alveolar basal epithelial cells) were seeded on 24-well plates in DMEM. Two wells were seeded with cells, one with a sensor and the other without. On day 1, 3 aliquots of MM (without phenylalanine, 10 μM phenylalanine, and 100 μM phenylalanine) were pre-equilibrated for 2 h in the incubator prior to EAB pH calibration in working buffer and phenylalanine calibration in MM. After calibration, the medium overlaying the cell monolayer was changed to MM (84 μM phenylalanine) and imaged by brightfield microscopy to ascertain morphology as a surrogate of cell biocompatibility of the measurement regime and to confirm the absence of microbial contamination. Real-time *in situ* measurements in cell culture commenced after a 3 h equilibration period and continued at hourly intervals for 72 h. The EAB sensor gold electrode was replaced daily by a fresh gold electrode, and each functionalized gold electrode was calibrated before submersion in the cell culture media. The utility of the EAB was evaluated in MRC-5 spheroids, with a 4 times higher cell number than the monolayer of A549 suspended in the same volume of Melbourne Media. The monolayer cell culture pH remained relatively stable over 72 h, and spheroid remained relatively stable over 24 h (Figure 5b), as independently confirmed by the pH paper measurement performed at the start and end of the cell culture (Figure S11). Phenylalanine levels, in contrast, declined, reflecting the use of this amino acid in support of cellular metabolism (Figure 5c). The spheroid shows a rapid phenylalanine clearance rate compared to monolayer cells (Figure 5c), whereas another tumor cell line, MDA-MB-231 (breast tumor), which is grown in monolayer culture, showed similar phenylalanine clearance to that of the A549 cell line (Figures S15 and S16). We compared the sensor-derived phenylalanine measurement against a GC−MS analysis. The ratio of phenylalanine concentration at day 1 (initial) of the monitoring to that at day 4 (final) was estimated, yielding a ratio of 0.42 based on EAB measurement compared with a ratio of 0.40 measured by GC−MS (Figure 5d and Table S4). Over the 4 days, there were no obvious changes in morphological appearance and no cell acridine orange/ethidium bromide (AO/EB)[59,60] viability assay differences in monolayer cell cultures between the two conditions (98.5% viability with sensor and 98.9% viability without sensor), confirming the biocompatibility of the sensor system (Figures 5e and S12, S13 and S17). Similarly, the MRC-5 spheroid over 1 day of measurement shows low cytotoxicity (Lactate Dehydrogenase (LDH) cytotoxicity assay[61] 6.3% of total LDH released into the supernatant) and no obvious morphological differences (Figures 5f and S14). Thus, the sensor provides continuous pH and phenylalanine measurements in cell culture with stability and reproducibility without cytotoxicity.

CONCLUSIONS

We have developed a miniaturized dual-purpose EAB sensor system to embed in conventional tissue culture plates for real-time studies. This sensor can simultaneously measure pH and the aptamer-target phenylalanine across the physiologically relevant ranges with good accuracy and precision. The sensor functions well in both static and flowing culture media. The integration of a leakless reference electrode into our dual-purpose EAB sensor system improved the whole system's stability, sterilizability, and biocompatibility. However, the system currently faces challenges related to biofouling and long-term stability, which must be addressed for extended applications. Applying an agarose hydrogel coating might mitigate biofouling by providing a barrier against biological material accumulation.[33] Our multiplexed sensor technology can be expanded into a multiaptamer dual-purpose EAB array for more comprehensive characterization of media in cell culture, including for microphysiological systems and organs on a chip.

MATERIALS AND METHODS

Materials and Reagents. The customized aptamer DNA oligo was obtained from Integrated DNA Technologies, Inc. (Coralville, IA, USA):

Phenylalanine aptamer sequence: /5ThioMC6-D/CG ACC GCG TTT CCC AAG AAA GCA AGT ATT GGT TGG TCG/3MeBIN/.[33]

Tryptophan aptamer sequence: /5ThioMC6-D/CC GGT GGT GTA GTT CCG GCG TGG GGA AGG/3MeBIN/.[47]

Doxorubicin aptamer sequence: /5ThioMC6-D/A CCA TCT GTG TAA GGG GTA AGG GGT GGT/3MeBIN/.[62]

Various equipment and materials were sourced from different suppliers:

Microliter syringe: Hamilton Company (Reno, Nevada, USA).

Autoclave machine PRATIKA B16-20: Siltex Pty Ltd. (Melbourne, Victoria, AU).

Microscope IX53: Olympus Corporation (Shinjuku City, Tokyo, Japan).

Potentiostat CHI1000C: CH Instruments (Austin, TX, USA).

Gold, platinum, and silver wires (200 μm diameter): Goodfellow Inc. (Huntingdon, UK).

Platinum wire (1 mm diameter), TE buffer, parafilm, TCEP, KH_2PO_4, Na_2HPO_4, NaCl, KCl, phenylalanine, tryptophan, doxorubicin, capillary glass tube, 6-mercapto-1-hexanol, heat-inactivated fetal calf serum (HIFCS), and penicillin−streptomycin solution: Sigma-Aldrich (Burlington, Massachusetts, USA).

PTFE head shrinking tube: McMaster-Carr Supply Company (Elmhurst, Illinois, USA).

Alligator Forma Series II Water-Jacketed CO_2 Incubator, NaOH, H_2SO_4, DMEM, NEAA, L-glutamine, phosphate-buffered saline (PBS), and CyQUANT LDH Cytotoxicity Fluorescence Assay: Thermo Fisher Scientific Australia (Waltham, Massachusetts, USA).

24-well plate: CoStar Group (Washington, District of Columbia, USA).

94-well plate: Corning Inc. (Corning, New York, USA).

Lonza MycoAlert Kit: Lonza Bioscience (Basel, Switzerland).

CLARIOstar microplate reader: BMG Labtech (Baden-Württemberg, Germany).

Eagle's minimum essential medium: American Type Culture Collection (ATCC) (Manassas, Virginia, USA).

Fabrication of Aptamer-Functionalized Gold Electrodes. The aptamer is bound to the gold electrode to register the electrochemical response to changes in the oligonucleotide structure that occur upon binding of the target metabolite. Fabrication requires resuspension of the oligonucleotide in TE buffer (Tris−EDTA) to 100 μM prior to storage at −20 °C until required. The gold wire (200 μm diameter) was cut to 4 cm and covered with a 3 cm PTFE tube, with one end having 3 mm bare for the aptamer coating and the other end having 7 mm bare for connection to the potentiostat. Then, the gold wire was electrochemically cleaned of residual organics through cyclic voltammetry pulses (−1 to −1.6 V for 1500 segments at a scan rate of 1 V/s in 0.5 M NaOH solution) and followed by electrochemical roughening (cyclic voltammetry pulses, 40 cycles between 0.35 and 1.6 V with a scan rate of 0.1 V/s, sample interval 0.001 s in 0.5 M H_2SO_4). Then, the reduced thiol-modified oligonucleotide (100 μM, 7 μL) was reacted in a solution of 14 μL of tris(2-carboxyethyl) phosphine (TCEP) (10 mM) at room temperature in the dark for 1 h. Then, the modified oligonucleotide was diluted to 500 nM in PBS,[33] and gold wire was immersed in this diluted 500 nM oligonucleotide solution at room temperature for 1 h

https://doi.org/10.1021/acsnano.4c06813
ACS Nano 2024, 18, 26127−26139

in the dark. After that, the gold wire was rinsed with distilled water and subsequently incubated in assembling buffer (5 mL containing 10 mM 6-mercapto-1-hexanol in PBS) overnight. These procedures were conducted within a sterile biosafety hood, and the PTFE tube-covered gold wire was sprayed with 80% ethanol before being moved into the biosafety hood.

Fabrication of Leakless Reference Electrodes. To fabricate the leakless reference electrode, a 3 mm platinum wire (200 μm diameter) was half inserted into the bottom end of a capillary glass tube (1 mm inner diameter) and sealed by a torch. Then, the capillary tube was filled with 3 M NaCl. Silver wire (200 μm diameter) was immersed in 1 M KCl and subjected to current of 1 mA/cm^2 for 10 min to create a Ag/AgCl-coated wire. The Ag/AgCl wire is then inserted into the top end of the capillary tube and sealed using parafilm and resin. The exposed Ag/AgCl wire from the capillary tube was secured with copper tape. The fabricated leakless refence electrode is stored in dark and dry conditions before use.

Fabrication of the 24-Well Sensor Lid. The sensor holder consists of two parts that were designed using AutoCAD and 3D printed in biocompatible resin in the Melbourne Centre of Nanofabrication. The screw component of the 3D printed holder (Figure S10a) was installed in a 24-well plate by drilling a 1 cm hole (Figure S10c) and was fixed by the nut component of the 3D printed holder (Figure S10b).

Preparation of Working Buffer. To prepare working buffer, NaCl, KCl, Na_2HPO_4, and KH_2PO_4 powder were weighed out into a 1 L measuring cylinder. The components were dissolved with 800 mL of Milli Q before topping up to 1 L to make a final concentration of 137 mM NaCl, 2.7 mM KCl, 10 mM Na_2HPO_4, and 1.8 mM KH_2PO_4. The prepared working buffer was then autoclaved, and the working buffer pH was adjusted by addition of 1 M NaOH or 1 M H_2SO_4 before use.

Titration in Working Buffer. To assess the sensitivity of the sensor to phenylalanine/tryptophan, gold electrodes are coated with phenylalanine-responsive/tryptophan-responsive aptamer. Then, 10 mM phenylalanine/tryptophan is dissolved in the working buffer, and solubility was confirmed by microscopic inspection. Then, 10 mM solution is serially diluted to 1 mM, 100 μM, 10 μM, and 1 μM solutions in working buffer. The aptamer-coated gold electrodes were removed from 10 mM 6-mercapto-1-hexanol and were rinsed with Mill-Q water before connecting to the potentiostat. After connecting three electrodes with potentiostat, the three electrodes were immersed in 14.985 mL of working buffer without phenylalanine/tryptophan in a 50 mL container. The SWV scanning was performed with signal-on frequencies (0.001 V step, 0.05 amplitude) and signal-off frequencies (0.003 V step, 0.05 amplitude) under a potential window −0.1 to −0.4 V. SWV was performed in multiple groups (usually around 50−80) in working buffer without phenylalanine/tryptophan until the peak current difference became stable. Then, the solution in a 50 mL container was titrated from 1 nM to 10 mM by adding phenylalanine/tryptophan solution to the working buffer. For each titration point, SWV was performed once.

Preparation of Melbourne Media. *Prepare Nutrition Stock Solutions.* Each powder or solid product was weighed out into a preweighed 50 mL Eppendorf tube by gently taping the bottle. The components were dissolved with an appropriate volume of solvent (calculated to achieve stock concentration), and 10 mL of the solutions were filtered with a 0.22 μm filter and 10 mL syringe into another marked 50 mL Eppendorf tube. The components are listed in Table S2.

Tyrode's Salt. Tyrode's salt powder was dissolved several times with a pipet with 10 mL of water for irrigation. The solution was added into a 50 mL container. The Tyrode's salt bag wall was rinsed with water for irrigation and was also added to the 50 mL container. Then, the solution was poured into a prepared 500 mL flask. The 50 mL container was rinsed several times with water for irrigation. Then, the 500 mL flask was topped up to around 300 mL.

Preparation of 2× Melbourne Media Base Solution. After obtaining the stock solutions of all products (Table S2), each of them (amino acids, essential nutrients, vitamins, buffering solutions) was added into the above-mentioned 500 mL flask (with Tyrode's salt solution added into it) according to the tabulated volumes and topped up to 400 mL. Then, 95 mL of water for irrigation was accurately added by pipet, and then 5.5 mL of 1 M NaOH solution was added.

Preparation of 1× Melbourne Media Solution. After preparation of 2× MM, 50 mL of 2× MM was aliquoted into one 200 mL sterile flask to prepare a final volume of 100 mL 1× MM, then the trace elements and supplements were added according to Table S3, and the solution was filtered into another 200 mL sterile flask. After that, the pH of 1× MM was adjusted to 7.2−7.4 with 1 M HCl or 1 M NaOH.

Titration in MM. First, phenylalanine was dissolved in 0.1 M HCl to make a 100 mM concentration. Then, the solution was serially diluted into MM with phenylalanine concentrations of: 10 mM, 1 mM, 300 μM, 100 μM, 30 μM, 10 μM, 1 μM, 100 nM, and 10 nM. Then, a 50 mL container was filled with sterilized 14 mL of MM and was pre-equilibrated in an incubator (37 °C, 5% CO_2) for 1 h before sensor electrode assembling. The titration was done via solution addition through a long silicon tube connected between the 50 mL container in the incubator and the syringe in an ambient environment. The syringe titration was achieved by using an external syringe pump. A 15 min equilibrium time was allowed before SWV scanning at each titration point.

Cell Maintenance. A549 adenocarcinoma-derived human alveolar basal epithelial cell line from the ATCC were cultured in DMEM phenol-red free stock solution supplemented with 0.2% (w/v) sodium bicarbonate, 100 IU/mL penicillin, 50 μg/mL streptomycin, and 15 mM 4(2hydroxyethyl)-1-piperazineethanesulfonic acid (HEPES). Cells were passaged in complete DMEM with 10% (v/v) heat-inactivated fetal bovine serum, 1 mM nonessential amino acids (NEAA), 2 mM glutamine, and 1 mM sodium pyruvate in a humidified incubator with 5% CO_2 at 37 °C. Mycoplasma testing was conducted routinely using the Lonza MycoAlert Kit to exclude contamination from all cell lines. A CLARIOstar plate reader was used to determine luminescence according to the manufacturer's instructions.

Cell Seeding. *A549 Cell Seeding.* Cells were seeded with density 100,000 cells/well (52,630 cells/cm^2) onto a flat-bottom 24-well plate. After 24 h, about 90% cell seeding confluency, the media was removed, washed once with PBS, replenished with serum-free MM, and imaged with the Olympus IX53 microscope before moving into the incubator for sensor measurements. A549 cells were used between passages 14−28.

MDA-MB-231 Cell Seeding. MDA-MB-231 cells were seeded with density 120,000 cells/well (62,176 cells/cm^2) onto a flat-bottom 24-well plate to allow attachment overnight and subsequently washed with PBS, and the medium was changed to MM in 24-well plates. After serum-free medium incubation for 24 h, the wells were imaged with an Olympus IX53 microscope before moving into an incubator for sensor measurement. MDA-MB-231 cells used in the experiments were between passages 25−32.

Generation of Fibroblast Spheroids. MRC-5 cells were cultured in ATCC-formulated Eagles' minimum essential medium (EMEM) supplemented with 10% HIFCS and 1% penicillin−streptomycin solution and kept in an incubator with 5% CO_2 at 37 °C.

For the experiments, cells from passage 10 were used. Cells were washed twice with PBS and detached with Trypsin (0.123%, v/v, in PBS) containing ethylenediaminetetraacetic acid (EDTA; 0.02% w/v). Cells were seeded at a density of 50,000 cells/well in 200 mL of EMEM containing 10% FCS and 1% penicillin−streptomycin ultralow attachment U-bottomed 96-well plates. Plates were subjected to centrifugation at 1000 RCF for 10 min to aggregate cells at the bottom of the wells. Cells were incubated at 37 °C and 5% CO_2 for 24 h to allow spheroids to form.

Microscopy. Optical microscopy was performed using the Olympus IX53 inverted microscope equipped with a 10× objective lens for the monolayer cell and a 4× objective lens for the spheroid. The image was taken from the center of each well in a 24-well plate. Imaging was conducted at room temperature. Image analysis was performed using ImageJ software (National Institutes of Health, USA).

https://doi.org/10.1021/acsnano.4c06813
ACS Nano 2024, 18, 26127−26139

Acridine Orange/Ethidium Bromide Staining. AO/EB[59,60] was used in combination with the Operetta High Content (Revvity) live cell imaging for viable and nonviable cell enumeration and automatic quantification of cell viability in 2D. Acridine orange and ethidium bromide solutions were mixed to create a 250 μg/mL working solution. 20 μL of the mixture of the working solution was added into the wells (1 mL medium/well) in the ratio of 1:50 (v/v). At the experimental end point, AO/EB stain was added at the final concentration of 5 μg/mL (reference level: 2−50 μg/mL). The plate was subject to centrifugation at 524 RCF for 5 min prior to assay as follows.

In the Operetta High Content Image System, temperature and CO_2 in the live chamber were maintained at 37 °C and 5% CO_2 level. We used 20×, 0.45NA Long WD objective lens, and the channels were set up as Acridine Orange (fluorescence excitation filter: 460−490, 50% excitation intensity, fluorescence emission filter: 500−550), ethidium bromide (fluorescence excitation filter: 520−550, fluorescence emission filter: 590−640), and bright field (50% transmission). Eighteen field areas per well were selected for imaging. Image analysis in Harmony software (Version 4.1, Revvity) was performed using a customized analysis pipeline. Total cells were detected from the sum channel of AO and EB. Viable/nonviable cells were classified according to the mean intensity of EB being under/over the threshold value, which was defined by observation of the images and the researcher's experience with the same cell line using positive (dead cells treated by 0.1% Triton X-100) and negative controls. Viable cell percentage was calculated as viable cell number divided by the total cell number

$$\text{viable cell percentage} = \frac{\text{viable cell number}}{\text{viable cell number} + \text{nonviable cell number}} \times 100$$

LDH Cytotoxicity Assay. LDH[61] release by spheroids was used as a measure of cell death. LDH release was assessed using the CyQUANT LDH Cytotoxicity Fluorescence Assay with minor adjustments to the manufacturer's protocol. All LDH assay kit reagents were made up and stored according to the manufacturer's instructions.

Cell culture supernatants were collected and centrifuged at 5000 RCF for 5 min, and 200 μL of the supernatant was transferred to a fresh tube. All eight spheroids from a control well were pooled and lysed using 5% Triton-X (AJAX, AJA1552-500 ML) and brief probe sonication in Melbourne Media to measure the maximal amount of LDH released by spheroids. Melbourne Media was used to determine the basal fluorescence. All samples were stored at −20 °C overnight. Samples were measured in triplicate wells using 50 μL per well in a 96-well black plate. 50 μL of the provided reaction mixture was added to each well and mixed gently by shaking, followed by a 10 min incubation in the dark. 50 μL of the provided stop solution was added, and the plate was read on CLARIOStar using an excitation wavelength of 560 nm and an emission wavelength of 590 nm.

The cytotoxicity was calculated using the following formula

$$\%\ \text{cytotoxicity} = \frac{\text{treated LDH activity}}{\text{maximum LDH acticity}} \times 100$$

Data Analysis. Data analysis and plotting were conducted using using a combination of Jupyter Notebook (version 6.4.5), Plotly (version 5.18.0), Python programming language (version 3.11.0), scikit-learn library, hillfit library, and the NumPy library.

Graphical Representation. Graphical representation of study findings was accomplished using Microsoft PowerPoint for the creation of group plots and illustrations. Parts of the experiment process and structural illustrations were drawn by using pictures from Servier Medical Art. Servier Medical Art by Servier is licensed under a Creative Commons Attribution 3.0 Unported License (https://creativecommons.org/licenses/by/3.0/).

ASSOCIATED CONTENT

Supporting Information

The Supporting Information is available free of charge at https://pubs.acs.org/doi/10.1021/acsnano.4c06813.

Tyrode's salt concentration; EAB sensor KDM calculation; GC−MS analyses steps; KDM response with multiple coatings; pH dependence measurement; phenylalanine dependence; and phenylalanine real-time measurements of A549 and spheroid with log−linear fit to t = 0 h (PDF)

AUTHOR INFORMATION

Corresponding Authors

Ranjith Rajasekharan Unnithan − *Department of Electrical and Electronic Engineering, University of Melbourne, Melbourne, Victoria 3010, Australia; ARC Centre for Personalised Therapeutics Technologies, Melbourne, Victoria 3010, Australia*; Email: r.ranjith@unimelb.edu.au

Alastair G. Stewart − *Department of Biochemistry and Pharmacology, University of Melbourne, Melbourne, Victoria 3010, Australia; ARC Centre for Personalised Therapeutics Technologies, Melbourne, Victoria 3010, Australia;* orcid.org/0000-0002-2271-5942; Email: astew@unimelb.edu.au

Authors

Yiling Yang − *Department of Electrical and Electronic Engineering, University of Melbourne, Melbourne, Victoria 3010, Australia; ARC Centre for Personalised Therapeutics Technologies, Melbourne, Victoria 3010, Australia;* orcid.org/0009-0001-1947-2791

Xumei Gao − *Department of Biochemistry and Pharmacology, University of Melbourne, Melbourne, Victoria 3010, Australia; ARC Centre for Personalised Therapeutics Technologies, Melbourne, Victoria 3010, Australia*

Bryce Widdicombe − *Department of Electrical and Electronic Engineering, University of Melbourne, Melbourne, Victoria 3010, Australia*

Xiaodan Zhang − *Department of Biochemistry and Pharmacology, University of Melbourne, Melbourne, Victoria 3010, Australia*

Jana Lorraine Zielinski − *Department of Biochemistry and Pharmacology, University of Melbourne, Melbourne, Victoria 3010, Australia;* orcid.org/0000-0002-6899-5564

Tianhong Cheng − *Department of Biochemistry and Pharmacology, University of Melbourne, Melbourne, Victoria 3010, Australia*

Avanka Gunatilaka − *Department of Biochemistry and Pharmacology, University of Melbourne, Melbourne, Victoria 3010, Australia*

Kaylyn K. Leung − *Department of Chemistry and Biochemistry, University of California Santa Barbara, Santa Barbara, California 93106, United States;* orcid.org/0000-0002-8966-801X

Kevin W. Plaxco − *Department of Chemistry and Biochemistry, University of California Santa Barbara, Santa Barbara, California 93106, United States;* orcid.org/0000-0003-4772-8771

Complete contact information is available at: https://pubs.acs.org/10.1021/acsnano.4c06813

https://doi.org/10.1021/acsnano.4c06813
ACS Nano 2024, 18, 26127−26139

Author Contributions

Y.Y. designed and conducted the research project and wrote the manuscripts; Y.Y., R.R.U., and A.G.S. conceived the idea; X.G. contributed to the sensor lid holder 3D printed design; X.Z. contributed to the preparation of Melbourne Medium, drafting Melbourne Medium protocol, and passaging, seeding, and AO/EB staining of MDA-MB-231 cells; J.L.Z. contributed to the passaging, seeding, and AO/EB staining of A549 cells; A.G. contributed to the generation of fibroblast spheroids and LDH assay. T.C. contributed to the GC−MS experiment and drafting the Melbourne Medium protocol; K.K.L. and K.W.P. provided support for EAB sensor fabrication; B.W., X.G., R.R.U., and A.G.S. guided experiment design and troubleshooting; R.R.U. and A.G.S. supervised the research; A.G.S. and K.W.P. edited the MS.

Funding

This work was supported by the Australian Research Council Centre for Personalized Therapeutics Technologies (grant no. IC170100016). This work was also supported by the National Health and Medical Research Council (grant no. 118637).

Notes

The authors declare no competing financial interest.

ACKNOWLEDGMENTS

This work was performed in part at the Melbourne Centre for Nanofabrication (MCN) in the Victorian Node of the Australian National Fabrication Facility (ANFF). Gas Chromatography Mass Spectrometry was performed in part at the Parkville Node of Metabolomics Australia. This work was also partially financially supported by the Graeme Clark Institute. The authors acknowledge that the technology described in this paper is covered by the provisional patent (AU 2023902007). We acknowledge the use of the Biological Optical Microscopy Platform (BOMP), University of Melbourne.

REFERENCES

(1) Sun, D.; Gao, W.; Hu, H.; Zhou, S. Why 90% of Clinical Drug Development Fails and How to Improve It? *Acta Pharm. Sin. B* **2022**, *12*, 3049−3062.

(2) Lefevre, I. A.; Balice-Gordon, R. J. Learning from Principles of Evidence-Based Medicine to Optimize Nonclinical Research Practices. In *Good Research Practice in Non-Clinical Pharmacology and Biomedicine*; Bespalov, A., Michel, M. C., Steckler, T., Eds.; *Handbook of Experimental Pharmacology*; Springer International Publishing: Cham, 2020; pp 35−54.

(3) Day, C.-P.; Merlino, G.; Van Dyke, T. Preclinical Mouse Cancer Models: A Maze of Opportunities and Challenges. *Cell* **2015**, *163*, 39−53.

(4) Edington, C. D.; Chen, W. L. K.; Geishecker, E.; Kassis, T.; Soenksen, L. R.; Bhushan, B. M.; Freake, D.; Kirschner, J.; Maass, C.; Tsamandouras, N.; Valdez, J.; Cook, C. D.; Parent, T.; Snyder, S.; Yu, J.; Suter, E.; Shockley, M.; Velazquez, J.; Velazquez, J. J.; Stockdale, L.; Papps, J. P.; Lee, I.; Vann, N.; Gamboa, M.; LaBarge, M. E.; Zhong, Z.; Wang, X.; Boyer, L. A.; Lauffenburger, D. A.; Carrier, R. L.; Communal, C.; Tannenbaum, S. R.; Stokes, C. L.; Hughes, D. J.; Rohatgi, G.; Trumper, D. L.; Cirit, M.; Griffith, L. G. Interconnected Microphysiological Systems for Quantitative Biology and Pharmacology Studies. *Sci. Rep.* **2018**, *8*, 4530.

(5) Ingber, D. E. Human Organs-on-Chips for Disease Modelling, Drug Development and Personalized Medicine. *Nat. Rev. Genet.* **2022**, *23*, 467−491.

(6) Low, L. A.; Mummery, C.; Berridge, B. R.; Austin, C. P.; Tagle, D. A. Organs-on-Chips: Into the next Decade. *Nat. Rev. Drug Discovery* **2021**, *20*, 345−361.

(7) Li, S.; Li, C.; Khan, M. I.; Liu, J.; Shi, Z.; Gao, D.; Qiu, B.; Ding, W. Microneedle Array Facilitates Hepatic Sinusoid Construction in a Large-Scale Liver-Acinus-Chip Microsystem. *Microsyst. Nanoeng.* **2023**, *9*, 75.

(8) Ma, L.-D.; Wang, Y.-T.; Wang, J.-R.; Wu, J.-L.; Meng, X.-S.; Hu, P.; Mu, X.; Liang, Q.-L.; Luo, G.-A. Design and Fabrication of a Liver-on-a-Chip Platform for Convenient, Highly Efficient, and Safe in Situ Perfusion Culture of 3D Hepatic Spheroids. *Lab Chip* **2018**, *18*, 2547−2562.

(9) Kim, J.; Lee, K.-T.; Lee, J. S.; Shin, J.; Cui, B.; Yang, K.; Choi, Y. S.; Choi, N.; Lee, S. H.; Lee, J.-H.; Bahn, Y.-S.; Cho, S.-W. Fungal Brain Infection Modelled in a Human-Neurovascular-Unit-on-a-Chip with a Functional Blood−Brain Barrier. *Nat. Biomed. Eng.* **2021**, *5*, 830−846.

(10) Park, J.; Lee, B. K.; Jeong, G. S.; Hyun, J. K.; Lee, C. J.; Lee, S.-H. Three-Dimensional Brain-on-a-Chip with an Interstitial Level of Flow and Its Application as an in Vitro Model of Alzheimer's Disease. *Lab Chip* **2015**, *15*, 141−150.

(11) Bai, H.; Si, L.; Jiang, A.; Belgur, C.; Zhai, Y.; Plebani, R.; Oh, C. Y.; Rodas, M.; Patil, A.; Nurani, A.; Gilpin, S. E.; Powers, R. K.; Goyal, G.; Prantil-Baun, R.; Ingber, D. E. Mechanical Control of Innate Immune Responses against Viral Infection Revealed in a Human Lung Alveolus Chip. *Nat. Commun.* **2022**, *13*, 1928.

(12) Benam, K. H.; Villenave, R.; Lucchesi, C.; Varone, A.; Hubeau, C.; Lee, H.-H.; Alves, S. E.; Salmon, M.; Ferrante, T. C.; Weaver, J. C.; Bahinski, A.; Hamilton, G. A.; Ingber, D. E. Small Airway-on-a-Chip Enables Analysis of Human Lung Inflammation and Drug Responses in Vitro. *Nat. Methods* **2016**, *13*, 151−157.

(13) Chou, D. B.; Frismantas, V.; Milton, Y.; David, R.; Pop-Damkov, P.; Ferguson, D.; MacDonald, A.; Vargel Bölükbaşı, Ö.; Joyce, C. E.; Moreira Teixeira, L. S.; Rech, A.; Jiang, A.; Calamari, E.; Jalili-Firoozinezhad, S.; Furlong, B. A.; O'Sullivan, L. R.; Ng, C. F.; Choe, Y.; Marquez, S.; Myers, K. C.; Weinberg, O. K.; Hasserjian, R. P.; Novak, R.; Levy, O.; Prantil-Baun, R.; Novina, C. D.; Shimamura, A.; Ewart, L.; Ingber, D. E. On-Chip Recapitulation of Clinical Bone Marrow Toxicities and Patient-Specific Pathophysiology. *Nat. Biomed. Eng.* **2020**, *4*, 394−406.

(14) Wagner, I.; Materne, E.-M.; Brincker, S.; Süßbier, U.; Frädrich, C.; Busek, M.; Sonntag, F.; Sakharov, D. A.; Trushkin, E. V.; Tonevitsky, A. G.; Lauster, R.; Marx, U. A Dynamic Multi-Organ-Chip for Long-Term Cultivation and Substance Testing Proven by 3D Human Liver and Skin Tissue Co-Culture. *Lab Chip* **2013**, *13*, 3538.

(15) Baert, Y.; Ruetschle, I.; Cools, W.; Oehme, A.; Lorenz, A.; Marx, U.; Goossens, E.; Maschmeyer, I. A Multi-Organ-Chip Co-Culture of Liver and Testis Equivalents: A First Step toward a Systemic Male Reprotoxicity Model. *Hum. Reprod.* **2020**, *35*, 1029−1044.

(16) Schimek, K.; Frentzel, S.; Luettich, K.; Bovard, D.; Rütschle, I.; Boden, L.; Rambo, F.; Erfurth, H.; Dehne, E.-M.; Winter, A.; Marx, U.; Hoeng, J. Human Multi-Organ Chip Co-Culture of Bronchial Lung Culture and Liver Spheroids for Substance Exposure Studies. *Sci. Rep.* **2020**, *10*, 7865.

(17) Esch, E. W.; Bahinski, A.; Huh, D. Organs-on-Chips at the Frontiers of Drug Discovery. *Nat. Rev. Drug Discovery* **2015**, *14*, 248−260.

(18) Fuchs, S.; Johansson, S.; Tjell, A.; Werr, G.; Mayr, T.; Tenje, M. In-Line Analysis of Organ-on-Chip Systems with Sensors: Integration, Fabrication, Challenges, and Potential. *ACS Biomater. Sci. Eng.* **2021**, *7*, 2926−2948.

(19) Shah, P.; Fritz, J. V.; Glaab, E.; Desai, M. S.; Greenhalgh, K.; Frachet, A.; Niegowska, M.; Estes, M.; Jäger, C.; Seguin-Devaux, C.; Zenhausern, F.; Wilmes, P. A Microfluidics-Based in Vitro Model of the Gastrointestinal Human−Microbe Interface. *Nat. Commun.* **2016**, *7*, 11535.

(20) Dolci, M.; Wang, Y.; Nooteboom, S. W.; Soto Rodriguez, P. E. D.; Sánchez, S.; Albertazzi, L.; Zijlstra, P. Real-Time Optical Tracking of Protein Corona Formation on Single Nanoparticles in Serum. *ACS Nano* **2023**, *17*, 20167−20178.

https://doi.org/10.1021/acsnano.4c06813
ACS Nano 2024, 18, 26127−26139

(21) Moya, A.; Ortega-Ribera, M.; Guimerà, X.; Sowade, E.; Zea, M.; Illa, X.; Ramon, E.; Villa, R.; Gracia-Sancho, J.; Gabriel, G. Online Oxygen Monitoring Using Integrated Inkjet-Printed Sensors in a Liver-on-a-Chip System. *Lab Chip* **2018**, *18*, 2023−2035.
(22) Misun, P. M.; Rothe, J.; Schmid, Y. R. F.; Hierlemann, A.; Frey, O. Multi-Analyte Biosensor Interface for Real-Time Monitoring of 3D Microtissue Spheroids in Hanging-Drop Networks. *Microsyst. Nanoeng.* **2016**, *2*, 16022.
(23) Dornhof, J.; Kieninger, J.; Muralidharan, H.; Maurer, J.; Urban, G. A.; Weltin, A. Microfluidic Organ-on-Chip System for Multi-Analyte Monitoring of Metabolites in 3D Cell Cultures. *Lab Chip* **2022**, *22*, 225−239.
(24) Idili, A.; et al. Continuous Monitoring of Molecular Biomarkers in Microfluidic Devices. In *Progress in Molecular Biology and Translational Science*; Academic Press, 2022; Vol. *187*, pp 295−333.
(25) Zirath, H.; Rothbauer, M.; Spitz, S.; Bachmann, B.; Jordan, C.; Müller, B.; Ehgartner, J.; Priglinger, E.; Mühleder, S.; Redl, H.; Holnthoner, W.; Harasek, M.; Mayr, T.; Ertl, P. Every Breath You Take: Non-Invasive Real-Time Oxygen Biosensing in Two- and Three-Dimensional Microfluidic Cell Models. *Front. Physiol.* **2018**, *9*, 815.
(26) Zhang, Y. S.; Aleman, J.; Shin, S. R.; Kilic, T.; Kim, D.; Mousavi Shaegh, S. A.; Massa, S.; Riahi, R.; Chae, S.; Hu, N.; Avci, H.; Zhang, W.; Silvestri, A.; Sanati Nezhad, A.; Manbohi, A.; De Ferrari, F.; Polini, A.; Calzone, G.; Shaikh, N.; Alerasool, P.; Budina, E.; Kang, J.; Bhise, N.; Ribas, J.; Pourmand, A.; Skardal, A.; Shupe, T.; Bishop, C. E.; Dokmeci, M. R.; Atala, A.; Khademhosseini, A. Multisensor-Integrated Organs-on-Chips Platform for Automated and Continual in Situ Monitoring of Organoid Behaviors. *Proc. Natl. Acad. Sci. U.S.A.* **2017**, *114*, E2293−E2302.
(27) Hu, X.-P.; Yang, Y.; Ma, B.-G. Amino Acid Flux from Metabolic Network Benefits Protein Translation: The Role of Resource Availability. *Sci. Rep.* **2015**, *5*, 11113.
(28) Eagle, H. Amino Acid Metabolism in Mammalian Cell Cultures. *Science* **1959**, *130*, 432−437.
(29) Masamha, C. P.; LaFontaine, P. Molecular Targeting of Glutaminase Sensitizes Ovarian Cancer Cells to Chemotherapy. *J. Cell. Biochem.* **2018**, *119*, 6136−6145.
(30) Højfeldt, J. W.; Helin, K. Regional Tumour Glutamine Supply Affects Chromatin and Cell Identity. *Nat. Cell Biol.* **2016**, *18*, 1027−1029.
(31) Xia, J.; Zhang, J.; Wu, X.; Du, W.; Zhu, Y.; Liu, X.; Liu, Z.; Meng, B.; Guo, J.; Yang, Q.; Wang, Y.; Wang, Q.; Feng, X.; Xie, G.; Shen, Y.; He, Y.; Xiang, J.; Wu, M.; An, G.; Qiu, L.; Jia, W.; Zhou, W. Blocking Glycine Utilization Inhibits Multiple Myeloma Progression by Disrupting Glutathione Balance. *Nat. Commun.* **2022**, *13*, 4007.
(32) Song, K.-M.; Lee, S.; Ban, C. Aptamers and Their Biological Applications. *Sensors* **2012**, *12*, 612−631.
(33) Idili, A.; Gerson, J.; Kippin, T.; Plaxco, K. W. Seconds-Resolved, In Situ Measurements of Plasma Phenylalanine Disposition Kinetics in Living Rats. *Anal. Chem.* **2021**, *93*, 4023−4032.
(34) Li, H.; Li, S.; Dai, J.; Li, C.; Zhu, M.; Li, H.; Lou, X.; Xia, F.; Plaxco, K. W. High Frequency, Calibration-Free Molecular Measurements in Situ in the Living Body. *Chem. Sci.* **2019**, *10*, 10843−10848.
(35) Li, S.; Dai, J.; Zhu, M.; Arroyo-Currás, N.; Li, H.; Wang, Y.; Wang, Q.; Lou, X.; Kippin, T. E.; Wang, S.; Plaxco, K. W.; Li, H.; Xia, F. Implantable Hydrogel-Protective DNA Aptamer-Based Sensor Supports Accurate, Continuous Electrochemical Analysis of Drugs at Multiple Sites in Living Rats. *ACS Nano* **2023**, *17*, 18525−18538.
(36) Dauphin-Ducharme, P.; Yang, K.; Arroyo-Currás, N.; Ploense, K. L.; Zhang, Y.; Gerson, J.; Kurnik, M.; Kippin, T. E.; Stojanovic, M. N.; Plaxco, K. W. Electrochemical Aptamer-Based Sensors for Improved Therapeutic Drug Monitoring and High-Precision, Feedback-Controlled Drug Delivery. *ACS Sens.* **2019**, *4*, 2832−2837.
(37) Idili, A.; Arroyo-Currás, N.; Ploense, K. L.; Csordas, A. T.; Kuwahara, M.; Kippin, T. E.; Plaxco, K. W. Seconds-Resolved Pharmacokinetic Measurements of the Chemotherapeutic Irinotecan in Situ in the Living Body. *Chem. Sci.* **2019**, *10*, 8164−8170.
(38) Chamorro-Garcia, A.; Gerson, J.; Flatebo, C.; Fetter, L.; Downs, A. M.; Emmons, N.; Ennis, H. L.; Milosavić, N.; Yang, K.; Stojanovic, M.; Ricci, F.; Kippin, T. E.; Plaxco, K. W. Real-Time, Seconds-Resolved Measurements of Plasma Methotrexate In Situ in the Living Body. *ACS Sens.* **2023**, *8*, 150−157.
(39) Gerson, J.; Erdal, M. K.; McDonough, M. H.; Ploense, K. L.; Dauphin-Ducharme, P.; Honeywell, K. M.; Leung, K. K.; Arroyo-Curras, N.; Gibson, J. M.; Emmons, N. A.; Meiring, W.; Hespanha, J. P.; Plaxco, K. W.; Kippin, T. E. High-Precision Monitoring of and Feedback Control over Drug Concentrations in the Brains of Freely Moving Rats. *Sci. Adv.* **2023**, *9*, No. eadg3254.
(40) Cheng, L.; Wang, X.; Liu, A.; Zhu, Y.; Cheng, H.; Yu, J.; Gong, L.; Liu, H.; Shen, G.; Liu, L. Phenylalanine Deprivation Inhibits Multiple Myeloma Progression by Perturbing Endoplasmic Reticulum Homeostasis. *Acta Pharm. Sin. B* **2024**, *14*, 3493−3512.
(41) Williams, R. A.; Mamotte, C. D.; Burnett, J. R. Phenylketonuria: An Inborn Error of Phenylalanine Metabolism. *Clin. Biochem. Rev.* **2008**, *29*, 31−41.
(42) Cleary, M.; Trefz, F.; Muntau, A. C.; Feillet, F.; van Spronsen, F. J.; Burlina, A.; Bélanger-Quintana, A.; Giżewska, M.; Gasteyger, C.; Bettiol, E.; Blau, N.; MacDonald, A. Fluctuations in Phenylalanine Concentrations in Phenylketonuria: A Review of Possible Relationships with Outcomes. *Mol. Genet. Metab.* **2013**, *110*, 418−423.
(43) Walker, N. L.; Dick, J. E. Leakless Bipolar Reference Electrodes: Fabrication, Performance, and Miniaturization. *Anal. Chem.* **2021**, *93*, 10065−10074.
(44) Arroyo-Currás, N.; Dauphin-Ducharme, P.; Ortega, G.; Ploense, K. L.; Kippin, T. E.; Plaxco, K. W. Subsecond-Resolved Molecular Measurements in the Living Body Using Chronoamperometrically Interrogated Aptamer-Based Sensors. *ACS Sens.* **2018**, *3*, 360−366.
(45) Ferguson, B. S.; Hoggarth, D. A.; Maliniak, D.; Ploense, K.; White, R. J.; Woodward, N.; Hsieh, K.; Bonham, A. J.; Eisenstein, M.; Kippin, T. E.; Plaxco, K. W.; Soh, H. T. Real-Time, Aptamer-Based Tracking of Circulating Therapeutic Agents in Living Animals. *Sci. Transl. Med.* **2013**, *5*, 213ra165.
(46) Downs, A. M.; Gerson, J.; Leung, K. K.; Honeywell, K. M.; Kippin, T.; Plaxco, K. W. Improved Calibration of Electrochemical Aptamer-Based Sensors. *Sci. Rep.* **2022**, *12*, 5535.
(47) Wu, Y.; Ranallo, S.; Del Grosso, E.; Chamoro-Garcia, A.; Ennis, H. L.; Milosavić, N.; Yang, K.; Kippin, T.; Ricci, F.; Stojanovic, M.; Plaxco, K. W. Using Spectroscopy to Guide the Adaptation of Aptamers into Electrochemical Aptamer-Based Sensors. *Bioconjugate Chem.* **2023**, *34*, 124−132.
(48) Psychogios, N.; Hau, D. D.; Peng, J.; Guo, A. C.; Mandal, R.; Bouatra, S.; Sinelnikov, I.; Krishnamurthy, R.; Eisner, R.; Gautam, B.; Young, N.; Xia, J.; Knox, C.; Dong, E.; Huang, P.; Hollander, Z.; Pedersen, T. L.; Smith, S. R.; Bamforth, F.; Greiner, R.; McManus, B.; Newman, J. W.; Goodfriend, T.; Wishart, D. S. The Human Serum Metabolome. *PLoS One* **2011**, *6*, No. e16957.
(49) Rifai, N., Horvath, A. R.; Wittwer, C. T. *Tietz Textbook of Clinical Chemistry and Molecular Diagnostics*, 6th ed.; Elsevier, 2018.
(50) Singhal, G. S.; Rabinowitch, E. Changes in the Absorption Spectrum of Methylene Blue with pH. *J. Phys. Chem.* **1967**, *71*, 3347−3349.
(51) Koutsoumpeli, E.; Murray, J.; Langford, D.; Bon, R. S.; Johnson, S. Probing Molecular Interactions with Methylene Blue Derivatized Self-Assembled Monolayers. *Sens. Bio-Sens. Res.* **2015**, *6*, 1−6.
(52) Deboux, B. J.-C.; Lewis, E.; Scully, P. J.; Edwards, R. A Novel Technique for Optical Fiber pH Sensing Based on Methylene Blue Adsorption. *J. Lightwave Technol.* **1995**, *13*, 1407−1414.
(53) González-Fernández, E.; Staderini, M.; Marland, J. R. K.; Gray, M. E.; Uçar, A.; Dunare, C.; Blair, E. O.; Sullivan, P.; Tsiamis, A.; Greenhalgh, S. N.; Gregson, R.; Clutton, R. E.; Smith, S.; Terry, J. G.; Argyle, D. J.; Walton, A. J.; Mount, A. R.; Bradley, M.; Murray, A. F. In Vivo Application of an Implantable Tri-Anchored Methylene Blue-Based Electrochemical pH Sensor. *Biosens. Bioelectron.* **2022**, *197*, 113728.

https://doi.org/10.1021/acsnano.4c06813
ACS Nano 2024, 18, 26127−26139

(54) Slawson, R. M.; Lee, H.; Trevors, J. T. Bacterial Interactions with Silver. *Biol. Met.* **1990**, *3*, 151−154.
(55) Ahamed, M.; Karns, M.; Goodson, M.; Rowe, J.; Hussain, S. M.; Schlager, J. J.; Hong, Y. DNA Damage Response to Different Surface Chemistry of Silver Nanoparticles in Mammalian Cells. *Toxicol. Appl. Pharmacol.* **2008**, *233*, 404−410.
(56) Greulich, C.; Braun, D.; Peetsch, A.; Diendorf, J.; Siebers, B.; Epple, M.; Köller, M. The Toxic Effect of Silver Ions and Silver Nanoparticles towards Bacteria and Human Cells Occurs in the Same Concentration Range. *RSC Adv.* **2012**, *2*, 6981.
(57) Wang, X.; Hao, Z.; Olsen, T. R.; Zhang, W.; Lin, Q. Measurements of Aptamer−Protein Binding Kinetics Using Graphene Field-Effect Transistors. *Nanoscale* **2019**, *11*, 12573−12581.
(58) Chen, Z.-M.; Mou, Q.; Wu, S.-H.; Xie, Y.; Salminen, K.; Sun, J.-J. Real-Time Tunable Dynamic Range for Calibration-Free Biomolecular Measurements with a Temperature-Modulated Electrochemical Aptamer-Based Sensor in an Unprocessed Actual Sample. *Anal. Chem.* **2022**, *94*, 1397−1405.
(59) Hague, A.; Manning, A. M.; Hanlon, K. A.; Hart, D.; Paraskeva, C.; Huschtscha, L. I. Sodium Butyrate Induces Apoptosis in Human Colonic Tumour Cell Lines in a P53-Independent Pathway: Implications for the Possible Role of Dietary Fibre in the Prevention of Large-Bowel Cancer. *Int. J. Cancer* **1993**, *55*, 498−505.
(60) Patsos, G.; Hebbe-Viton, V.; Robbe-Masselot, C.; Masselot, D.; Martin, R. S.; Greenwood, R.; Paraskeva, C.; Klein, A.; Graessmann, M.; Michalski, J. C.; Gallagher, T.; Corfield, A. O-Glycan Inhibitors Generate Aryl-Glycans, Induce Apoptosis and Lead to Growth Inhibition in Colorectal Cancer Cell Lines. *Glycobiology* **2009**, *19*, 382−398.
(61) Kumar, P.; Nagarajan, A.; Uchil, P. D. Analysis of Cell Viability by the Lactate Dehydrogenase Assay. *Cold Spring Harb. Protoc.* **2018**, *2018*, pdb.prot095497.
(62) Arroyo-Currás, N.; Somerson, J.; Vieira, P. A.; Ploense, K. L.; Kippin, T. E.; Plaxco, K. W. Real-Time Measurement of Small Molecules Directly in Awake, Ambulatory Animals. *Proc. Natl. Acad. Sci. U.S.A.* **2017**, *114*, 645−650.

https://doi.org/10.1021/acsnano.4c06813
ACS Nano 2024, 18, 26127−26139